JOURNAL OF MATERIALS SCIENCE 32 (1997) 4575–4583

Microstructural characterization of surface layers formed on a low alloy steel during erosion – oxidation in a fluidized bed

P. M. ROGERS, I. M. HUTCHINGS, J. A. LITTLE*
Department of Materials Science and Metallurgy, University of Cambridge, Pembroke Street, Cambridge, CB2 3QZ, UK

F. KARA
Department of Ceramics, Engineering Faculty, Anadolu University, Yunusemre Kampüsü, 26470 Eskisehir, Turkey

Low alloy steel specimens were subjected to erosion-oxidation in a simulated fluidized bed environment in the range 100–600° C. Transmission electron microscopy was carried out on the surfaces which experienced particle impacts, with specimens prepared by backthinning. At low temperatures ($\leqslant 200^\circ$C) a dense, protective layer of bed particle fragments formed on the steel surface due to fragmentation of particle asperities and their subsequent comminution to a very fine size (<10 nm). At intermediate temperatures thin oxide films developed on the wear scar surfaces; these were predominantly magnetite with a fine grain size. There was rapid material loss with particle impacts removing the oxide and some metal below, but the thin oxide rapidly regrew due to the fine grain size, absence of a hæmatite layer and the mechanical damage during particle impact. At high temperatures the oxide became sufficiently thick to be mechanically protective. Erosion occurred within the fine grained surface hæmatite layer, while there was grain growth in the lower magnetite layer.

1. Introduction

High temperature erosion/abrasion-corrosion problems can occur in gas turbines, fluidized bed coal combustors (FBCs), catalytic crackers, coal gasifiers and sinter-crushers. A protective oxide scale may form on the surface of the metallic components in such systems, but the situation becomes even more complex when the component surface is also subjected to mechanical attack by particles. In this case the surface oxide may be continuously removed, causing rates of material loss considerably greater than those occurring during solely either oxidation or erosion.

Simulations of the conditions experienced in gas turbines, with high particle impact velocities have indicated that the exact behaviour and the resulting morphology of the metal surface depends on the severity of erosion and the oxidation rate (Fig. 1) [1, 2]. *Pure erosion of the oxide* dominates at high temperatures where the oxidation rate is high, while *pure erosion of metal* occurs at low temperature. In the *erosion-enhanced oxidation* regime a steady-state oxide thickness develops, with the rate of oxide formation equal to the rate of scale removal by erosion. When the erosion rate is high compared with the scaling rate, the *oxidation-affected erosion* regime is entered and under these conditions a continuous oxide scale is unable to form and the metal surface comprises a composite layer of oxide, embedded erodent fragments and extruded metal.

In a bubbling fluidized bed combustor, coal is burnt in a bed of inert particles (such as silica sand and ash) which is fluidized by air fed in from below. A calcium-based sorbent (e.g., limestone or dolomite) may also be fed into the bed to reduce emissions of sulphur oxides. The bed material may thus contain sand, ash and reacted (or partially reacted) sorbent [3]. During operation, a high flux of particles strikes the inbed heat exchanger tubing at low velocity in a manner which may be described as a combination of 3-body abrasion and erosion. Although the particle size, flux and velocity in a FBC are significantly different from gas turbine conditions, the regimes of behaviour discussed above may still be relevant.

The environment in an FBC has been simulated in a laboratory rig in which specimens attached to a vertical shaft were moved through an electrically heated fluidized bed of particles. The shaft was rotated at constant angular velocity so that the particle impact velocity and flux increased along the length of the

* Author to whom all correspondence should be sent.

0022–2461

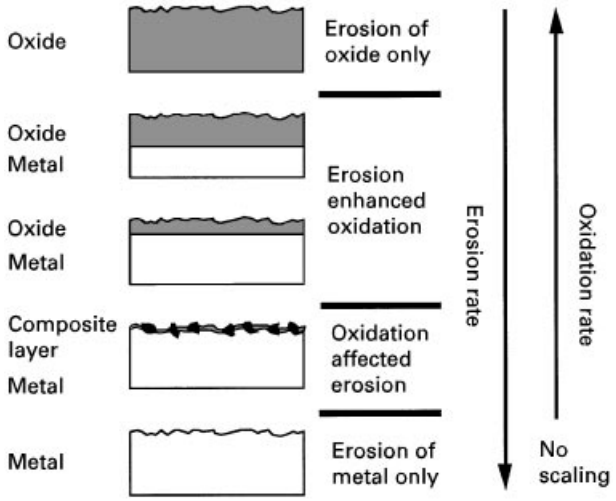

Figure 1 Erosion–corrosion regimes, after Kang *et al.* [1].

horizontal specimens [4]. Various steels were tested in this apparatus; maximum material loss was typically observed at intermediate temperatures (300–500° C), with less wastage at lower and higher temperatures [5, 6].

Rogers *et al.* examined the surface microstructures which developed on a low alloy steel (722M24T) after erosion-oxidation in this apparatus [7]. At 100 and 200° C, a continuous layer of embedded bed particle fragments formed on the specimen, providing mechanical protection so that negligible material loss occurred from these regions. High levels of wastage occurred at 300 and 400° C, possibly by the regular removal and regrowth of the thin oxide films, exhibiting optical interference colours, which developed over the wear scars. A thin interference-coloured oxide also developed over the wear scar at high velocities at 500° C, but at lower velocities there was a transition to a thicker grey oxide which was cratered. At 600° C a thicker grey oxide, which was also cratered, formed along the whole wear scar length; this oxide was sufficiently thick to provide mechanical protection against particle impacts and the wastage therefore decreased.

In the present work, transmission electron microscopy (TEM) was used to examine further the microstructures of the wear scars developed on 722M24T steel in the study described above. This technique was particularly useful in view of the fine scale of the microstructure which had been identified in the earlier work [7]. Although scanning electron microscopy (SEM) has regularly been used to examine erosion–corrosion microstructures, TEM studies have been rare, particularly on specimens with well-characterized histories from laboratory studies.

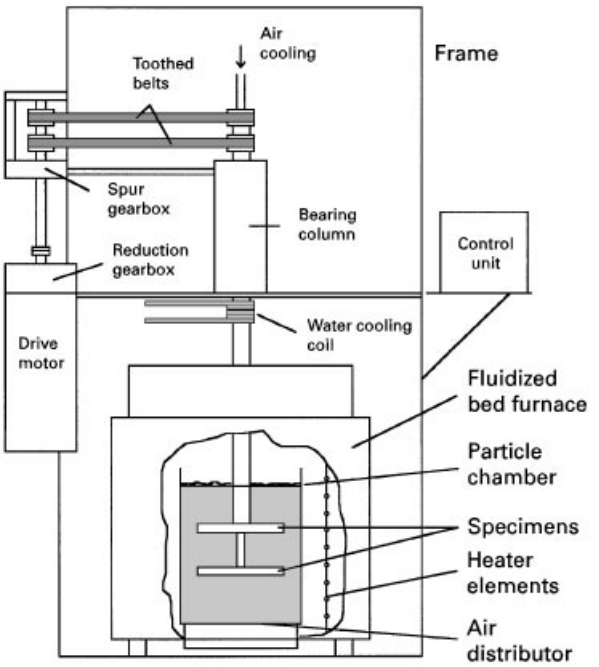

Figure 2 Laboratory test apparatus used for erosion–corrosion studies.

2. Experimental procedure

The erosion–corrosion test apparatus (Fig. 2) was built around an electrically-heated fluidized bed. The particle chamber contained angular alumina particles with an average diameter of 240 μm, as measured by laser granulometry. The particles were used in a conditioned state, achieved by regularly removing a small quantity from the bed and replacing it with fresh material [4]. During tests, the air flow-rate into the bed was adjusted to give a light fluidization condition.

The 722M24T steel test specimens (for composition see Table 1) were prepared in the form of solid cylinders, 80 mm long and 25 mm in diameter, with a ground and polished surface finish. These were mounted on coaxial vertical shafts and were rotated in a horizontal plane immersed in the fluidized bed. The upper pair of specimens was rotated in an opposite sense to the lower to minimize gross stirring of the bed. The tangential velocity increased radially along the specimen length from 0.5 to 2.6 m s^{-1}, with a range of particle impact angles around the front half of the specimen due to its cylindrical shape [4–7]. The steel had a hardness of 300 kgf mm^{-2} H_V and a microstructure consisting of fine lower bainitic laths up to 25 μm long.

Experiments were carried out at various temperatures, each for a duration of 72 h. The brief time (a

TABLE I Composition of 722M24T steel

	Composition (wt%)									
Steel	Fe	C	Cr	Mo	Si	Mn	S	P	Ni	Cu
722M24T	bal	0.28	3.33	0.47	0.27	0.45	0.034	0.012	0.20	0.23

few minutes) taken to remove the specimens from the hot fluidized bed furnace led to some oxide growth on the wear scar during this period of static oxidation. Wastage was measured as the maximum reduction in specimen radius and was determined by precision metrology at a number of positions along the specimen length (i.e., at several effective particle impact velocities) [7]. The regions which showed significant material loss or particle embedment were on the front half of the circumference, on either side of the specimen leading edge (Fig. 3). A "dead zone" of defluidized particles is believed to press against the leading edge during exposure in the rig and this prevents the wear scar extending to angles closer to the front. A graph of wastage against temperature determined in this way for 722M24T steel is shown in Fig. 4.

Regions from the wear scars of the erosion–corrosion specimens were sectioned with a SiC slitting wheel in order to prepare samples for TEM. The samples were prepared by back-thinning of the specimen except for the sample tested at 100° C which had a sufficiently thick surface deposit (≈ 3 μm) to permit preparation of an edge-on specimen. Samples were ground and polished to a thickness of 50 μm and dimpled (with a Gatan Dimple Grinder).The dimpling was carried out to minimize the ion beam milling time, since longer milling times resulted in the build-up of a layer of contamination over the face of the specimen. TEM was performed with Philips 400 ST and 400 T (with Energy Dispersive X-ray (EDX) spectroscopy) microscopes, both operated at 120 kV.

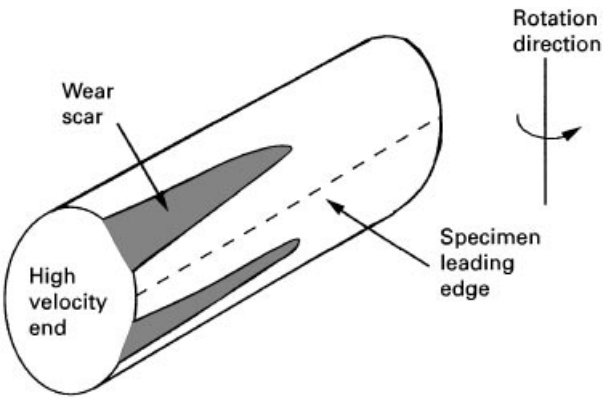

Figure 3 Schematic diagram of a worn sample.

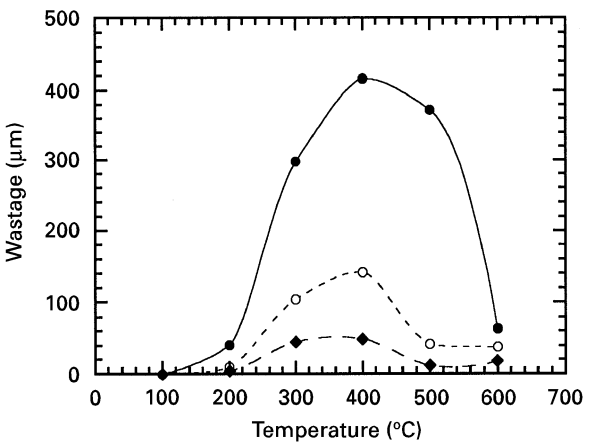

Figure 4 Graph of wastage against temperature for 722M24T steel after an exposure time of 72 h. Key: (●) 2.5 m s^{-1}, (○) 2.0 m s^{-1} and (◆) 1.7 m s^{-1}.

3. Results

3.1. Microstructure developed at 100°C

A cross-section of the continuous alumina deposit which formed over the specimen leading surface at 100° C is shown in Fig. 5. The alumina layer was up to 5 μm thick, being strongly adherent, with negligible porosity and comprizing embedded fragments too fine to be resolved by scanning electron microscopy. Below the deposit there was some evidence of shear deformation of the substrate in the direction of the particle flow (from right to left in this micrograph). Examination of the substrate/deposit interface by TEM showed that the bainite laths had been sheared parallel to the interface (Fig. 6). The microstructure of the deposit is shown in Fig. 7, in dark-field imaging conditions and exhibits a very fine alumina fragment size (typically 5–10 nm), but with occasional larger pieces a few hundred nanometres in diameter.

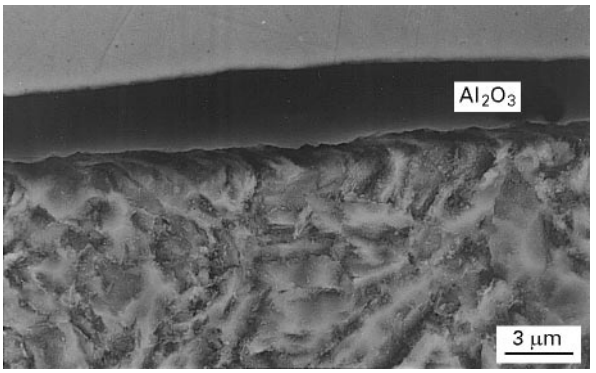

Figure 5 SEM backscattered electron image of a cross-section through a sample of 722M24T steel exposed at 100° C and 2.4 m s^{-1} (substrate etched in 2% nitric acid in ethanol).

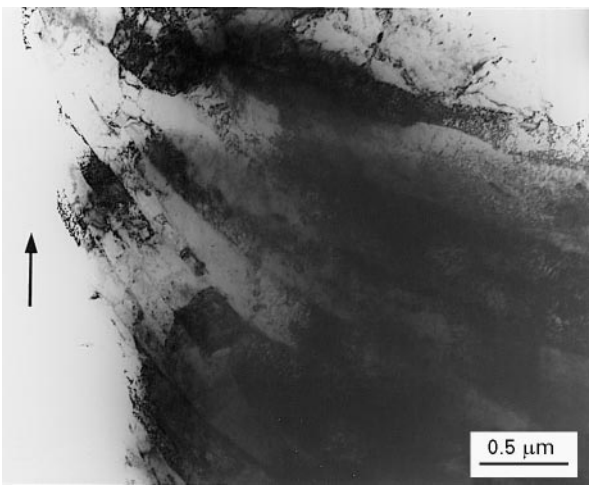

Figure 6 TEM bright field image showing the bending of ferrite laths at the substrate/deposit interface for 722M24T steel exposed at 100° C. (Note the alumina deposit in this region of the cross-sectional specimen was ion milled preferentially.)

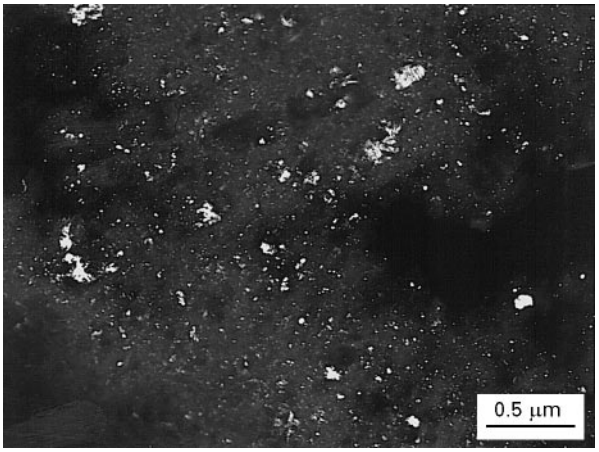

Figure 7 TEM dark field image of the alumina deposit formed on the surface of 722M24T steel exposed at 100° C (back-thinned specimen).

3.2. Microstructure developed at 200° C

Bed particle fragments were also deposited over much of the front half of the specimen at 200° C, although narrow wear scars did develop at locations corresponding to glancing particle impact [7]. Fig. 8 shows a bright field TEM micrograph of a back-thinned specimen from the wear scar. Both oxide (region B) and substrate material (region A) can be identified, suggesting that the oxide film was very thin and possibly discontinuous in places. The diffraction pattern for region A shows some rings due oxide as well as the metal. The oxide structure was identified as a spinel, probably magnetite, with an oxide grain size which varied from 15 nm in some areas, to as fine as 2 nm in other regions. Fig. 9(a–c) is a schematic diagram showing the first rings of the diffraction patterns for iron, magnetite (Fe_3O_4), and hæmatite (Fe_2O_3) to the same scale as used for the diffraction patterns of the micrographs.

3.3. Microstructure developed at 300° C

A dark-field image (Fig. 10) and the associated diffraction patterns show that the oxide film which developed at 300° C (region A) consisted mainly of magnetite (with a grain size of about 10 nm), and a small amount of hæmatite. Only the substrate steel

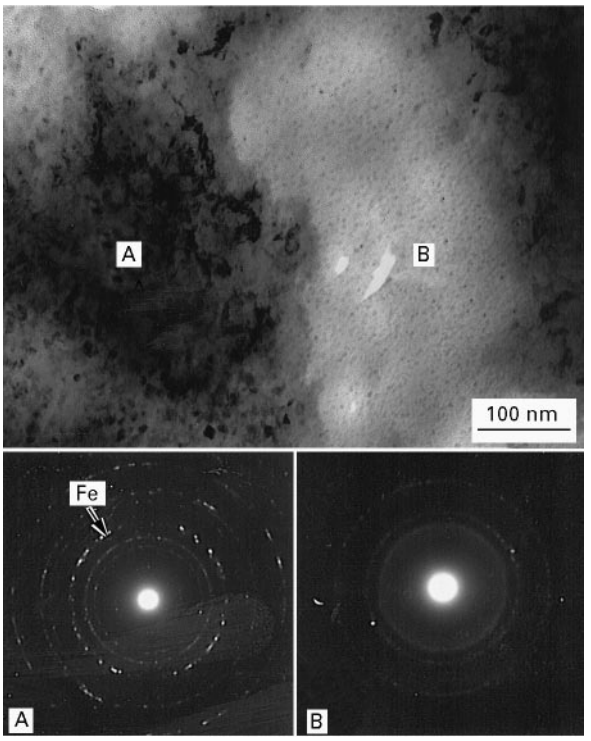

Figure 8 TEM bright field image of a back-thinned specimen of the wear scar for 722M24T steel exposed at 200° C showing discontinuous oxide on the surface. Region A corresponds to the steel substrate and region B to the spinel oxide.

appeared to be imaged in certain areas (region B), also suggesting that the surface oxide was discontinuous but, when present, the oxide was thicker than at 200° C. Although diffraction patterns from regions A and B show both oxide and metal diffraction rings, the dark field image indicates distinct regions of fine oxide grains and others showing just larger metal grains.

Earlier studies in which specimen surfaces were examined by scanning electron microscopy showed that at intermediate temperatures discrete, submicrometre alumina fragments became embedded in the wear scar [7, 8]. A discrete agglomerate of particle fragments is shown in Fig. 11 in the region indicated by the arrows. The agglomerate was a few hundred nanometres in size and similar fragments were observed at all temperature where a thin oxide film covered the wear scar (i.e., in the regime of oxidation-affected erosion). The streaking of the spots in the

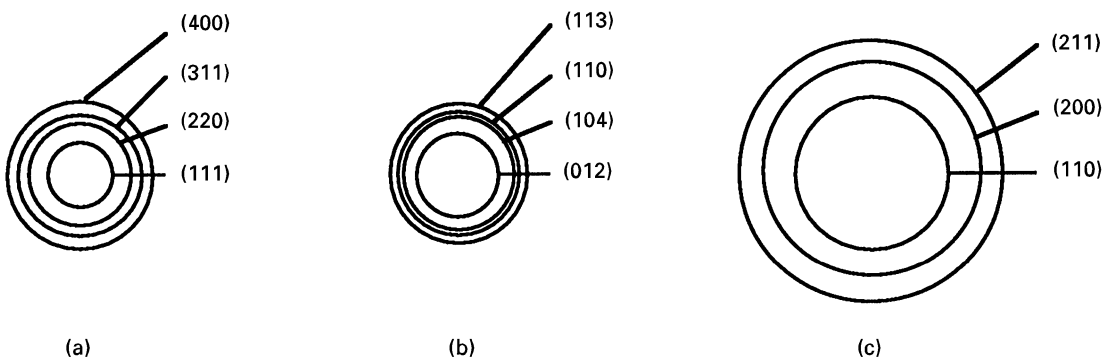

Figure 9 Schematic diagram showing the first main rings of the diffraction patterns for (a) magnetite (b) hæmatite and (c) iron.

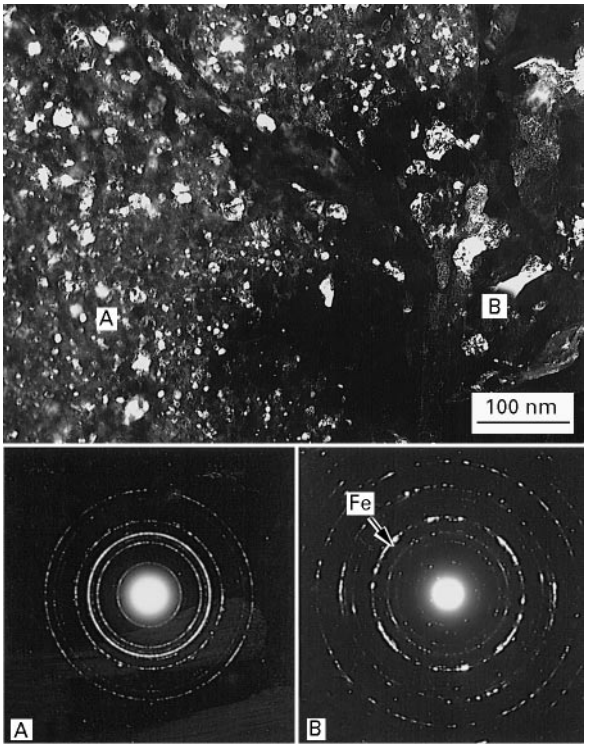

Figure 10 TEM dark field image of a back-thinned specimen of the wear scar for 722M24T steel exposed at 300° C showing discontinuous oxide on the surface. Region A is oxide (magnetite with some hæmatite) while region B is steel substrate.

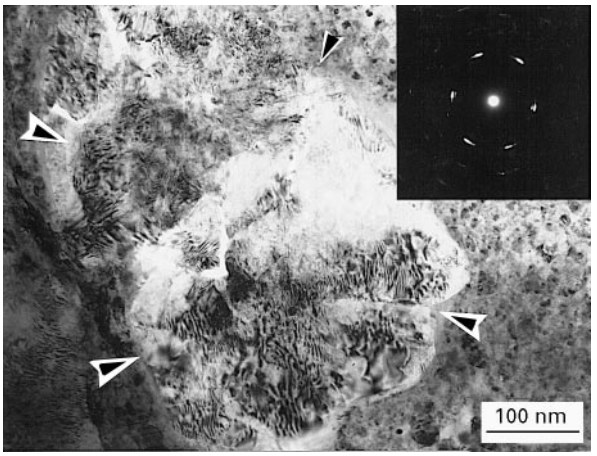

Figure 11 TEM bright field image of 722M24T steel exposed at 300° C showing an alumina fragment embedded in the surface of the wear scar with oxide and steel also present. The diffraction pattern is of the alumina fragments.

diffraction pattern indicates that the alumina fragments had been deformed.

3.4. Microstructure developed at 400° C

The oxide which developed at 400° C was thicker and continuous, so that individual islands of metal were no longer observed in the back-thinned sample (Fig. 12). The diffraction pattern indicated that the oxide was magnetite, although iron was also identified in the diffraction pattern in thicker regions which were still electron transparent (< 100 nm). Many of the oxide grains were 30–40 nm in diameter, but finer grains

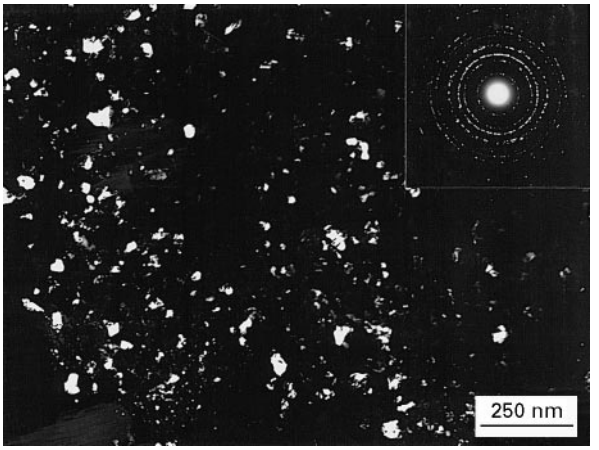

Figure 12 TEM dark field image of 722M24T steel exposed at 400° C showing the oxide on the wear scar.

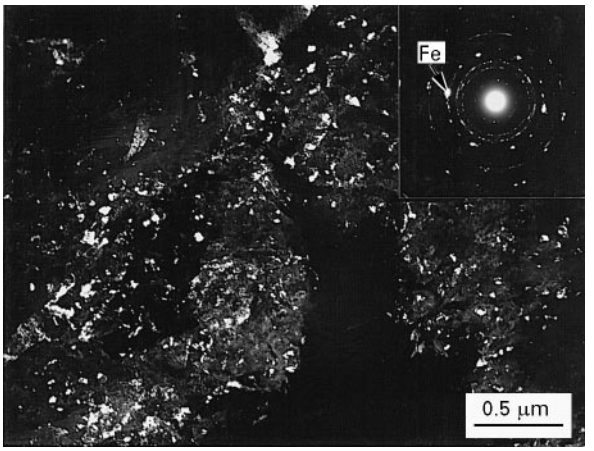

Figure 13 TEM dark field image of the oxide formed on 722M24T steel statically oxidized for 10 min at 400° C.

(≈5 nm) were also present. EDX analysis of the oxide showed it to have a similar chromium concentration to the substrate.

For comparison, a sample of 722M24T steel was oxidized statically by heating at 400° C in air for 10 min. The oxide film formed under these conditions is shown in Fig. 13 and had a grain size which varied between 15–50 nm. Diffraction analysis showed that the oxide was mainly magnetite, with a small amount of hæmatite also being present. Iron was also clearly present, which suggested that the statistically-formed oxide may be thinner than the film which was formed over the wear scar by erosion–corrosion at 400° C.

3.5. Microstructure developed at 500° C

At the high velocity end of the specimen, a thin interference-coloured oxide film formed over the wear scar (oxidation-affected erosion) [7]. Fig. 14 (a bright field image) shows this oxide to be predominantly magnetite, with some grains ≈50 nm in diameter and others ≈3 nm. Small amounts of hæmatite were noted in some regions, but iron was not detected, indicating that the oxide film formed at 500° C was thicker than that formed at 400° C.

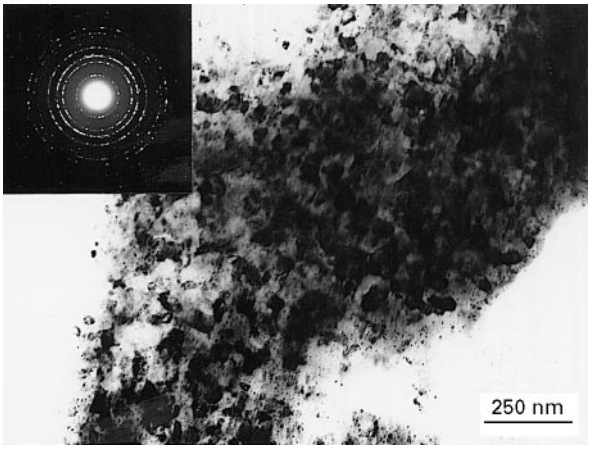

Figure 14 TEM bright field image of 722M24T steel exposed at 500° C showing the oxide on the wear scar at higher velocities.

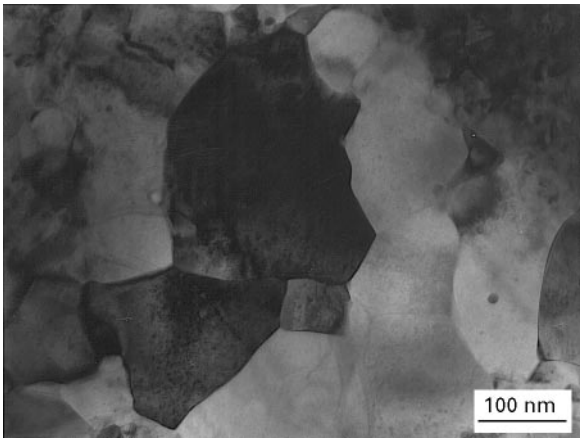

Figure 16 TEM bright field image of 722M24T steel exposed at 500° C showing the larger magnetite oxide grains formed in the scale at lower velocities.

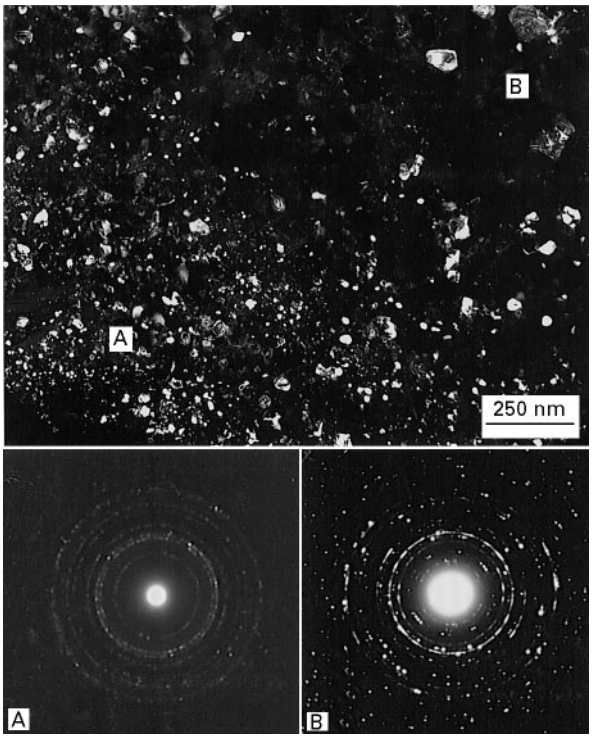

Figure 15 TEM dark field image of 722M24T steel exposed at 500° C showing the thicker oxide formed on the wear scar at lower velocities. Region A and the diffraction pattern are of the hæmatite grains, while region B and the diffraction pattern are of the magnetic grains.

At lower velocities a thicker, grey oxide scale which was cratered formed over the wear scar (now in the regime of erosion-enhanced oxidation) [7]. Fig. 15 shows this scale with a region of hæmatite (A) of grain size between 5–50 nm and an area of magnetite grains (B) between 100–300 nm in diameter. Fig. 16 is a bright field image of the magnetite grains, which are seen to be equiaxed with negligible porosity or cracks. The hæmatite grains were observed at the edge of the back-thinned specimen, indicating that the hæmatite layer was located at the top of the scale as would be expected. Occasionally there were magnetite regions with no hæmatite above them, perhaps caused by the removal of the upper layer by particle impact. Discrete embedded alumina fragments were also found in this thicker oxide exposed at lower velocities.

4. Discussion

4.1. Bed material deposits

In a FBC boiler an ash-based deposit may form on in-bed heat exchanger tubing at metal temperatures greater than $\approx 500^\circ$ C [9]. The composition of the deposit is related to that of the mineral phases fed into the combustor, and when a sorbent is used the deposit tends to be rich in $CaSO_4$ (anhydrite). The microstructure is dense and compacted, with a grain size of $\approx 1\,\mu$m. The mechanism of ash deposit formation in FBCs involves sintering of fine ash particles ($< 10\,\mu$m) deposited on the tube surface. Condensation of alkali metal compounds such as Na_2SO_4 can add to the deposit and encourage greater particle deposition (by assisting the adhesion of bed particles), while particle impact aids compaction of the deposit [9].

Deposits or embedded layers of bed particle fragments have also been noted in laboratory simulations of an FBC environment. The apparatus used by MacAdam and Stringer at Berkeley [10] contained a horizontal cylindrical specimen, submerged in a minimally fluidized bed, which was periodically thrust a short distance downwards and then slowly pulled upwards. Deposits formed on specimens during both room temperature [10–12] and elevated temperature exposure in this apparatus [13].

In the current work, significant deposition of bed particle fragments occurred only at temperatures of 200° C and below. In this case the continuous deposit was up to 5 μm thick and consisted predominantly of alumina bed particle fragments of 5–10 nm in diameter, with occasional larger alumina fragments (≈ 100 nm). In the study by MacAdam and Stringer, the surface layer formed on aluminium specimens at room temperature in a quartz bed [11] was somewhat different. The layer was up to 30 μm thick and consisted of alternating fine layers of deposited submicrometre silica debris and highly strained metallic foils, with the foils aligned in the direction of the particle flow during the downward specimen strokes.

Cold-worked, flattened platelets have been observed at the interface between the substrate and the oxide/deposit over worn areas on some steel FBC boiler tubes [14, 15]. Although no metallic foils or lamellar features were apparent within the deposit in this study, particle impacts had caused deformation of the substrate (at the interface with the deposit) in the direction of particle flow. The lower damage to the substrate in this case may be due to the lower particle mass (and kinetic energy) employed in these experiments.

The bed particles used in the Berkeley experiments [11] were reported to have numerous small fragments on their surfaces, resulting from comminution of the bed particles. These fragments were transferred to the specimen during impact, and the nature of the fragments was believed to influence strongly the morphology of the wear scar and the wear rate. In elevated temperature studies with abrasive grade quartz, MacAdam and Stringer noted significant quantities of fragments on the surface of the particles, such that, under conditions which allowed more fine dust in the bed, abrasive particles became partially encased in a layer of agglomerated quartz fragments [13]. Transfer of agglomerated fragments from the particle surface to the specimen encouraged the formation of a surface deposit, which could then result in a reduction in the wastage rate.

Attrition of the quartz bed particles was significant in the Berkeley apparatus, particularly at elevated temperatures. In early studies at Cambridge, 240 μm silica sand particles were used as the bed material but, at elevated temperatures, rapid fragmentation of the particles occurred [16]. The alumina particles used in the present study experienced considerably less attrition, although small quantities of fine dust formed on the surface of the fluidized bed, particularly at lower temperatures. Unlike the quartz particles used in the Berkeley studies, the alumina particles used in the present work were found not to be contaminated by fine fragments on their surface.

It can therefore be concluded that the alumina deposits observed in the current work probably resulted from the detachment of asperities during impact between particle and specimen. These fragments were responsible for the occasional larger alumina particles (a few hundred nanometres in diameter) in the deposit; although subsequent impacts leave more fragments they will probably also cause consolidation and fracture of the particles already present in the deposit. Repeated impacts will cause further fracture and plastic deformation of the fragments, forming the dense, fine grained deposit shown in Fig. 7.

It is possible that alumina deposition may predominate at lower temperatures because alumina is more brittle at such temperatures, and will therefore have a greater tendency to form fragments on impact. Some evidence for this hypothesis is provided by the greater formation of dust within the bed at lower bed temperatures and the absence of significant deposition in other studies carried out at a higher bed temperature ($\geqslant 300^\circ$ C), but with the specimen cooled internally to metal temperatures of 200° C and below [8, 17, 18]. Some variation in the transition temperature occurs with specimen material between bed particle deposition and the formation of a thin oxide film on the wear scar. This may be partly associated with the hardness of the substrate, with less deposition occurring on harder substrates. Impacting particles imbeded less deeply into harder specimens and smaller fragments from the asperities then remained in the surface. Oxidation may also play a role in inhibiting significant deposition, with the formation of iron oxide possibly lowering the adhesion between the fragment and the substrate or between fragments.

In FBC boilers the wastage of in-bed heat exchanger tubing falls significantly once the metal temperature is sufficiently high [19]. This has usually been attributed to the formation of a surface oxide thick enough to be mechanically protective, but the development of a deposit on the surface also discourages wastage in FBCs [3]. In the current work little wastage occurred at the low temperatures at which deposition occurred. This differs from the deposition behaviour found in practice, but does demonstrate the importance of deposition in laboratory tests as well as in FBC boilers. The type of deposit which forms in laboratory tests is likely to depend on factors such as the bed material (hardness and fracture behaviour), the specimen (hardness and oxidation rate) and the bed temperature (which effects the brittleness of the particles).

4.2. Oxides formed during erosion–corrosion

It has been shown that Fe_3O_4 (magnetite) forms on iron during the initial stages of static oxidation at temperatures between 220–500° C [20, 21]. The film grows rapidly until a layer of Fe_2O_3 (hæmatite) develops over its surface causing a substantial reduction in the oxidation rate. The nucleation rate of hæmatite increases with partial pressure of oxygen (pO_2) and so the period of rapid oxidation before hæmatite formation is smaller at higher pO_2. Studies of the early stages of oxidation of Fe–5 wt % Cr have revealed that magnetite was the only phase to form during the first ten minutes exposure at 600° C in 1 atmosphere (1.013×10^5 Pa) of oxygen [22].

The oxide films which developed on the wear scars between 200–500° C in the present erosion-oxidation studies were thin, being continually removed and then regrowing. The oxide film was thus always in the early stages of growth and proved to be largely magnetite as expected. Without a surface layer of hæmatite, the magnetite would be expected to grow rapidly. In addition, the very fine oxide grain size would have enhanced the outward diffusion of iron along the grain boundaries. Studies of the initial oxidation kinetics of mild steel at temperatures between 350–600° C have shown that the oxidation rate over the first few minutes is an order of magnitude greater than the rate at later times [18]. Particle impacts would additionally result in plastic deformation, fracture of the film and the combination of these effects would be expected to result in a sharply enhanced initial oxidation rate.

At 200° C, deposition of bed particle fragments predominated over much of the specimen surface but, in a narrow region of the specimen corresponding to near-glancing particle incidence, wastage was detected [7]. TEM showed the surface to be covered with a thin, probably discontinuous layer of magnetite, suggesting that lateral growth to form a continuous layer of magnetite was still occurring. Particles striking the surface in this area at such oblique angles were less likely to leave embedded fragments but were able to remove a region of oxide and underlying metal.

The thin interference-coloured oxides which formed on the wear scars between 300–500° C were largely magnetite and fine-grained, and therefore fast growing. Particles impinging on the surface removed oxide and metal during contact and left fine fragments of alumina ($\approx$100 nm in diameter) embedded in the metal surface; the clean surface then rapidly re-oxidized. Embedment of fragments probably did not result in the formation of a continuous layer since the particles were less brittle which reduced the fragmentation, while oxidation of the metal may have reduced adhesion of the fragments to the specimen.

The thickness of oxide removed by particle contact increased with temperature, while the extent of damage to the metal substrate decreased. At 300° C the oxide was still somewhat discontinuous, and so deformation and removal of metal itself played an important role. At 400° C a thicker and continuous oxide formed over the wear scar; particle impacts caused removal of this thicker oxide which was brittle, and also caused some damage to ductile metal below. The surface oxide was still thicker at 500° C, and the particle impacts may not have been sufficiently energetic to remove the whole oxide layer; the wastage rate therefore decreased.

At lower impact velocities at 500° C a duplex scale developed which was thick enough to become mechanically protective. A fine grained layer of hæmatite was able to nucleate at the surface and particle impacts removed oxide largely from this layer. The grains in the lower layer of magnetite were therefore able to coarsen (Figs 15 and 16).

5. Conclusions

Erosion–corrosion is a complex process in which, depending on the conditions, the behaviour may be dominated by erosion in the metal itself, oxidation-affected erosion, erosion enhanced-oxidation, erosion of the surface oxide or particle fragment deposition. In a fluidized bed environment the wastage rate may be reduced when conditions allow a mechanically protective oxide or deposit to form.

The current work used transmission electron microscopy to characterize the surface layers formed on 722M24T steel during laboratory erosion-oxidation tests at temperatures between 100–500° C. At 200° C and below, a mechanically protective dense deposit of alumina bed particle fragments up to 5 μm thick formed on the steel surface. This layer was probably formed by the fracture of particle asperities during impact with the specimen and the subsequent comminution of these fragments to a very fine size. The deposition behaviour is likely to depend on the nature of the bed particles, the specimen surface and the bed temperature.

High wastage rates occurred at intermediate temperatures, at which a thin Fe_3O_4 (magnetite) layer formed on the wear scar surface. Material was lost by the removal of the surface oxide and through some plastic deformation of the underlying ductile metal. The oxidation rate (and therefore material loss rate) was high, due to the rapid growth of magnetite in the absence of a surface layer of Fe_2O_3 (hæmatite). The very fine oxide grain size allowed enhanced grain boundary diffusion, and the mechanical damage and the resulting plastic deformation also enhanced diffusion.

At high temperatures, the oxide became thick enough to be mechanically protective and duplex layers of hæmatite and magnetite were formed. Erosion occurred predominantly in the upper hæmatite and magnetite were formed. Erosion occurred predominantly in the upper hæmatite layer (with a fine grain size) which allowed grain growth to occur in the magnetite layer.

Acknowledgements

This work was funded by the UK Engineering and Physical Sciences Research Council. The authors thank Dr N. J. Simms at the Coal Technology Development Division, Cheltenham for helpful discussions.

References

1. C. T. KANG, F. S. PETTIT and N. BIRKS, *Metall. Trans. A* **18** (1987) 1785.
2. S. L. CHANG, F. S. PETTIT and N. BIRKS, *Oxidation Met.* **34** (1990) 23.
3. J. STRINGER, S. S. MacADAM, I. G. WRIGHT and V. K. SETHI, *J. de Physique IV* **3** (1993) 797.
4. A. J. NINHAM, M. J. ENTWISLE, I. M. HUTCHINGS and J. A. LITTLE, Proceedings of the 10th International Conference on Fluidized Bed Combustion, San Francisco CA, April 1989, edited by A. M. Manaker (ASME, New York, 1989) pp. 583–590.
5. A. J. NINHAM, I. M. HUTCHINGS and J. A. LITTLE, *Corrosion* **46** (1990) 296.
6. P. M. ROGERS, T. E. HOWES, I. M. HUTCHINGS and J. A. LITTLE, *Wear* **186–187** (1995) 306.
7. P. M. ROGERS, I. M. HUTCHINGS and J. A. LITTLE, *ibid* **154** (1992) 269.
8. P. M. ROGERS, *PhD dissertation*, University of Cambridge, (1992).
9. J. E. OAKEY, A. J. MINCHENER and J. STRINGER, *J. Inst. Energy* **62** (1989) 208.
10. S. S. MacADAM and J. STRINGER, *Wear* **135** (1990) 403.
11. *Idem*, *ibid* **169** (1993) 141.
12. Y. LIU and A. V. LEVY, *ibid* **151** (1991) 365.
13. S. S. MacADAM and J. STRINGER, *Corrosion* **49** (1993) 156.
14. C. E. WITHERELL and R. G. MEISENHEIMER, in EPRI Workshop Proceedings, Wastage of In-Bed Surfaces in Fluidized-Bed Combustors, Argnne IL, November 1987, Paper 5.11.
15. C. E. WITHERELL, in Proceedings of the 10th International Conference on Fluidized Bed Combustion, San Francisco CA, April 1989, edited by A. M. Manaker (ASME, New York, 1989) pp. 937–944.

16. M. J. ENTWISLE, *PhD dissertation*, University of Cambridge, (1990).
17. T. E. HOWES, P. M. ROGERS, J. A. LITTLE and I. M. HUTCHINGS, *Wear* **186–187** (1995) 316.
18. T. E. HOWES, *PhD dissertation*, University of Cambridge, (1996).
19. G. J. HOLTZER and P. L. F. RADEMAKERS, in Proceedings of the 11th International Conference on Fluidized Bed Combustion, Montréal, April 1991, edited by E. J. Anthony (ASME, New York, 1991) pp. 743–753.
20. W. E. BOGGS, R. H. KACHIK and G. E. PELLISSIER, *J. Electrochem. Soc.* **112** (1965) 539.
21. C. I. HOWE, B. McENANEY and V. D. SCOTT, *Corrosion Science* **25** (1985) 195.
22. B. CHATTOPADHYAY and G. C. WOOD, *J. Electrochem. Soc.* **117** (1970) 1163.

Received 26 July 1996
and accepted 21 March 1997